CFD ANALYSIS OF HELICAL NOZZLES EFFECTS ON THE ENERGY SEPARATION IN A VORTEX TUBE

by

Nader POURMAHMOUD*[1], Amir HASSAN ZADEH[1], Omid MOUTABY[1], Abdolreza BRAMO[1]

[1]Department of Mechanical Engineering, Urmia University, Urmia, Iran
E-mail: n.pormahmod@urmia.ac.ir
E-mail: st_a.hassanzadeh@urmia.ac.ir
E-mail: omid_8102229@yahoo.com
E-mail: rezabramo@yahoo.com

In this article computational fluid dynamics (CFD) analysis of a three-dimensional steady state compressible and turbulent flow has been carried out through a vortex tube. The numerical models use the k–ε turbulence model to simulate an axisymmetric computational domain along with periodic boundary conditions. The present research has focused on the energy separation and flow field behavior of a vortex tube by utilizing both straight and helical nozzles. Three kinds of nozzles set include of 3 and 6 straight and 3 helical nozzles have been investigated and their principal effects as cold temperature difference was compared. The studied vortex tubes dimensions are kept the same for all models. The numerical values of hot and cold outlet temperature differences indicate the considerable operating role of helical nozzles, even a few numbers of that in comparing with straight nozzles. The results showed that this type of nozzles causes to form higher swirl velocity in the vortex chamber than the straight one. To be presented numerical results in this paper are validated by both available experimental data and flow characteristics such as stagnation point situation and the location of maximum wall temperature as two important facts. These comparisons showed reasonable agreement.

Key words: Vortex tube, CFD simulation, Stagnation point, Energy separation, Helical nozzles

1. Introduction

Vortex tube is also known as the Ranque-Hilsch vortex tube is a mechanical device that separates compressed air (or any inert gas) into hot and cold streams. The vortex tube was invented in 1933 by French physicist George J. Ranque [1]. Physicist Rudolf Hilsch improved the design and published a widely read paper in 1947 on the device [2]. A vortex tube has no moving part, and only compressed air is injected tangentially into one or more nozzles, which causes the air to rotate at a high speed. It rotates and moves towards the end of the vortex tube. Using of a conical valve at the end of tube lets exiting of hot gas and then formation of reversely rotating vortex moving in opposite direction. This flow is forced to return in an inner vortex of reduced diameter within the outer vortex, and exit through the central orifice near the entrance nozzles; that is called cold exit. This mechanism is described in fig. 1.

Kurosaka [3] reported the temperature separation to be a result of acoustic streaming effect

Figure 1. Schematic drawing of a vortex tube operational mechanism

that transfers energy from the cold core to the hot outer annulus. Stephan *et al.* [4] proposed the formation of Gortler vortices on the inside wall of the vortex tube that drive the fluid motion. Ahlborn and Gordon [5] described an embedded secondary circulation. Aljuwayhel *et al.* [6] utilized a fluid dynamics model of the vortex tube to understand the process that drives the temperature separation phenomena. Behera *et al.* [7] used the CFD to simulate the flow field and energy separation. Skye *et al.* [8] used a model similar to that of Aljuwayhel *et al.* [6]. Chang *et al.* [9] conducted a visualization experiment using surface tracing method to investigate the internal flow phenomena and to indicate the stagnation position in a vortex tube. Eisma *et al.* [10] performed a numerical study to research the flow field and temperature separation phenomenon. Volkan Kirmaci [11] applied Taguchi method to optimize the number of nozzle of vortex tube. Akhesmeh *et al.* [12] made a CFD model in order to study the variation of velocity, pressure and temperature inside a vortex tube. Their results obtained upon numerical approach comprehensively emphasized on the mechanism of hot peripheral flow and a reversing cold inner core flow formation. Xue Y. *et al.* [13] discussed on pressure, viscosity, turbulence, temperature, secondary circulation and acoustic streaming. Bramo and Pourmahmoud [14-16] studied numerically the effect of length to diameter ratio (L/D) and stagnation point occurrence importance in flow patterns. Hossein Nezhad and Shamsoddini [17] based on a three dimensional CFD model analyzed the mechanism of flow and heat transfer in the vortex tube.

Until now, complete understanding of the physical mechanisms that occurs in the vortex tube is one of the most scientific challenges in theoretical and experimental researches. Recent efforts that have successfully benefited of CFD could explain the basic principles behind the energy separation produced by the vortex tube. More designing parameters such as tube length and its geometry, cold and hot exit area, number of nozzles can be governed the flow field behavior in a vortex tube. But among them, nozzle geometrical shape is a specific case because it can be significantly enhanced the entrance gas velocity to vortex chamber. The present investigation, therefore, tends to explore the effects of helical nozzle geometry as a one of the main fundamentals of vortex tube structure in describing energy separation and clarification of correlation between stagnation point location and the position where the maximum wall temperature occurs.

2. Governing equations

The compressible turbulent and highly rotating flow inside the vortex tube is assumed to be three-dimensional, steady state and employs the standard k-ε turbulence model. The *RNG* k-ε turbulence model and more advanced turbulence models such as the Reynolds stress equations were also investigated, but as known these models could not be made to converge for this simulation. Bramo and Pourmahmoud [15] showed that, because of good agreement of numerical results with the experimental data, the k-ε model can be selected to simulate the effect of turbulence inside of computational domain. Consequently, the governing equations are arranged by the conservation of mass, momentum and energy equations, which are given by:

$$\frac{\partial}{\partial x_j}(\rho u_j)=0 \tag{1}$$

$$\frac{\partial}{\partial x_j}(\rho u_i u_j)=-\frac{\partial p}{\partial x_i}+\frac{\partial}{\partial x_j}\left[\mu\left(\frac{\partial u_i}{\partial x_j}+\frac{\partial u_j}{\partial x_i}-\frac{2}{3}\delta_{ij}\frac{\partial u_k}{\partial x_k}\right)\right]+\frac{\partial}{\partial x_j}(-\rho\overline{u_i'u_j'}) \tag{2}$$

$$\frac{\partial}{\partial x_i}\left[u_i\rho\left(h+\frac{1}{2}u_j u_j\right)\right]=\frac{\partial}{\partial x_j}\left[k_{eff}\frac{\partial T}{\partial x_j}+u_i(\tau_{ij})_{eff}\right], \qquad k_{eff}=K+\frac{c_p\mu_t}{\mathrm{Pr}_t} \tag{3}$$

Since we assumed the working fluid is an ideal gas, then the compressibility effect must be imposed so that:

$$p=\rho RT \tag{4}$$

The turbulence kinetic energy (k) and the rate of dissipation (ε) are got from the following equations:

$$\frac{\partial}{\partial t}(\rho k)+\frac{\partial}{\partial x_i}(\rho k u_i)=\frac{\partial}{\partial x_j}[(\mu+\frac{\mu_t}{\sigma_k})\frac{\partial k}{\partial x_j}]+G_k+G_b-\rho\varepsilon-Y_M \tag{5}$$

$$\frac{\partial}{\partial t}(\rho k)+\frac{\partial}{\partial x_i}(\rho k u_i)=\frac{\partial}{\partial x_j}[(\mu+\frac{\mu_t}{\sigma_\varepsilon})\frac{\partial \varepsilon}{\partial x_j}]+C_{1\varepsilon}\frac{\varepsilon}{k}(G_k+C_{3\varepsilon}G_b)-C_{2\varepsilon}\rho\frac{\varepsilon^2}{k} \tag{6}$$

In these equations, G_k, G_b, and Y_M represent the generation of turbulence kinetic energy due to the mean velocity gradients, the generation of turbulence kinetic energy due to buoyancy and the contribution of the fluctuating dilatation in compressible turbulence to the overall dissipation rate, respectively. $C_{1\varepsilon}$ and $C_{2\varepsilon}$ are constants. σ_k and σ_ε are the turbulent prandtel numbers for k and ε also. The turbulent (or eddy) viscosity, μ_t, is computed as follows:

$$\mu_t=\rho C_\mu\frac{k^2}{\varepsilon} \tag{7}$$

Where, C_μ is a constant. The model constants $C_{1\varepsilon}$, $C_{2\varepsilon}$, C_μ, σ_k and σ_ε have the following default values: $C_{1\varepsilon}$ = 1.44, $C_{2\varepsilon}$ = 1.92, C_μ = 0.09, σ_k = 1.0, σ_ε = 1.3.

3. Vortex tube model description

The CFD models of present research are based on the analysis of Skye *et al*. [8] experimental vortex tube. The vortex tube had been equipped with 6 straight nozzles. In an experimental and numerical analysis process, they found a good correlation between two approaches, however their

CFD model has employed 2D computational model. Since the high rotating flow inside the vortex tube makes a complex compressible turbulent flow, therefore one must be analyzed these types of flow patterns in full 3D CFD models. Bramo and Pourmahmoud [14-16] enhanced capability of Skye *et al.* [8] model results in 3D CFD models, so that this system has been investigated in with respect to various geometrical parameters such as tube length. The exploration of stagnation point location showed that the experimental device tube length was just appropriately, as the numerical results prediction.

Hence, this article has devoted its research direction to study effects of both nozzles number and its geometry on the mentioned device. In the new regarding, the Skye's vortex tube is modeled numerically with respect to 3 straight and 3 helical nozzles instead of 6 straight nozzles such that the total nozzles area are kept constant to all set of nozzles. This is due to the fact that this article believes that helical nozzles can play very considerable role in appropriately operating of a vortex tube even for a few number of nozzles in comparison with straight nozzles.

As the geometry of the vortex tube is periodic, only a part of sector is taken for analysis in given cyclic boundary condition. Basic assumptions for all computations of the particular vortex tube flows were made as follows: A circumferential pressurized gas inlet and two axial orifices for cold and hot stream with air as a working fluid. Since the chamber consists of 3 slots, the CFD models are assumed to be a rotational periodic flow and only a sector of the flow domain with angle 120° needs to be considered. The 6 straight nozzles CFD model corresponds to Skye's experimental vortex tube is shown in fig. 2. Figure 3 describes introduced 3D CFD vortex tube models with 3 straight and 3 helical nozzles. Dimensional geometric details of these models are presented in tab. 1.

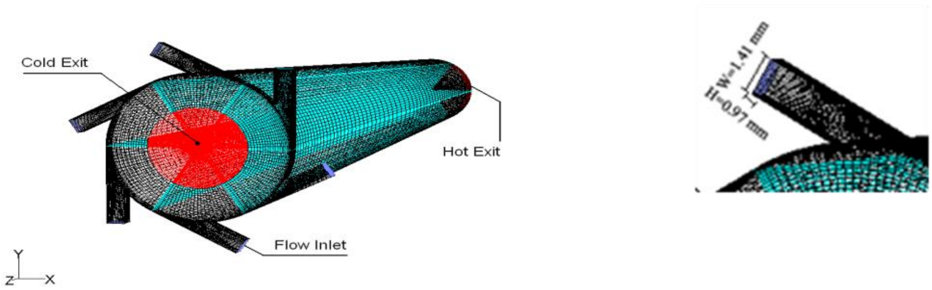

(a) (b)

Figure 2. a) 3D CFD model of vortex tube with six straight nozzles b) nozzles geometrical details

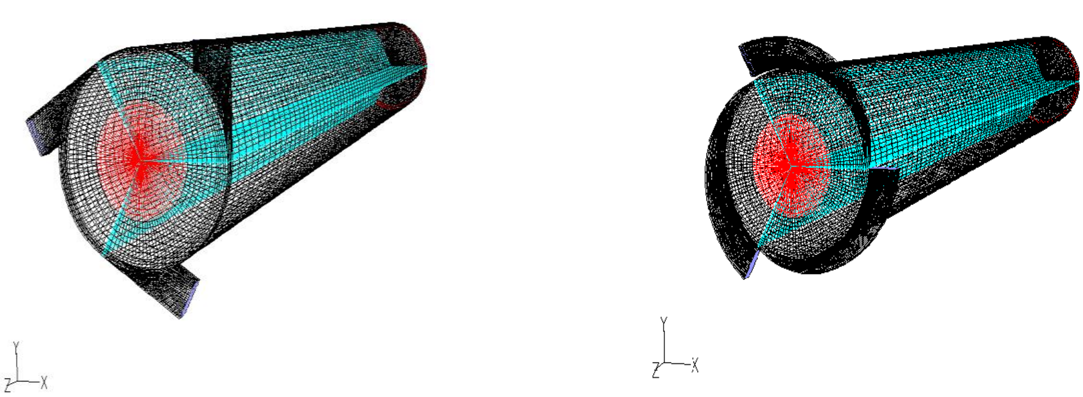

(a) (b)

Figure. 3: 3D modified CFD model of vortex tube with a) 3 straight nozzles b) 3 helical nozzles

Boundary conditions for the models are determined based on the experimental measurements by Skye *et al.* [8]. The inlet is modeled as a mass flow inlet. The specified total mass flow rate and stagnation temperature are fixed to 8.35 gr/s and 294.2 K, respectively. The static pressure at the cold exit boundary was fixed at experimental measurements pressure. The static pressure at the hot exit boundary is adjusted in the way to vary the cold mass fraction.

Table 1: Geometric summery of CFD models used for vortex tube

Measurement	Skye's experimental vortex tube	Present vortex tube with 3 number of either helical or straight nozzle
Working tube length	106 mm	106 mm
Working tube I.D.	11.4 mm	11.4 mm
Nozzle height	0.97 mm	0.97 mm
Nozzle width	1.41 mm	2.82 mm
Nozzle total inlet area(A_n)	8.2 mm^2	8.2 mm^2
Cold exit diameter	6.2 mm	6.2 mm
Hot exit area	95 mm^2	95 mm^2

3.1 Validation

A compressible form of the Navier-Stokes equations together with appropriate k-ε turbulence model are derived and solved by using the FLUENT™ software package. In order to discretise of derivative terms, the second order upwind and quick schemes are employed to momentum, turbulence and energy equations. The temperature separation obtained from the present calculations were compared with the experimental results of Skye *et al.*[8] for validation. Figures 4 and 5 show the cold and hot temperature differences. As seen in fig. 4, the cold temperature difference ($\Delta T_{i,c}$) predicted by the model is in good agreement with the experimental results. Prediction of the cold exit temperature difference is found to lie between the experimental and computational results of Skye *et al.* [8]. However, both numerical results of hot exit temperature difference ($\Delta T_{i,h}$) are very closer to experimental data as shown in fig. 5.

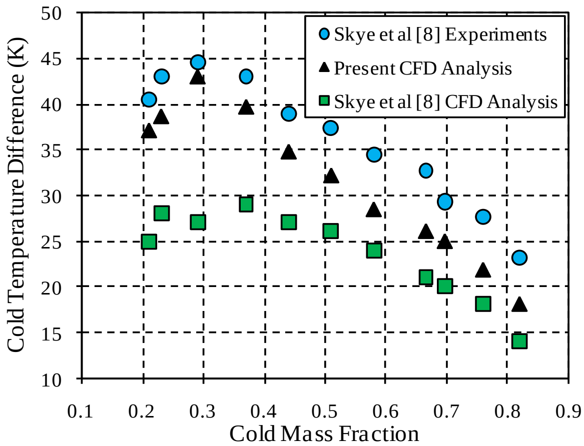

Figure 4. Cold exit temperature difference as a function of cold mass fraction

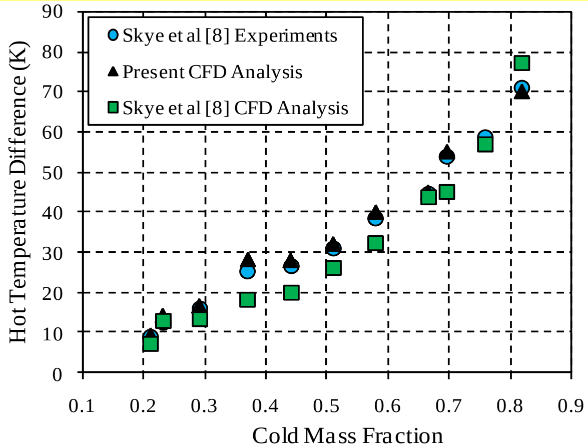

Figure 5. Hot exit temperature difference as a function of cold mass fraction

The hot exit temperature difference is observed to increase with an increase in the cold mass fraction. The maximum hot exit temperature difference of 70 K was found due to a cold mass fraction of 0.81. Meanwhile in cold mass fraction range of 0.2–0.4, the cold temperature differences can reach to its maximum values.

4. Results and discussion

4.1 Effect of nozzles shape

In vortex tube, shape type and number of inlet nozzles are quite important. So far, many investigations have been implemented on these parameters to achieve the best performance of vortex tube upon minimum cold outlet temperature. Kirmaci and Uluer [18] investigated the vortex tube performance experimentally. They used 2, 3, 4, 5 and 6 numbers of nozzles with air inlet pressures varying from 150 kPa to 700 kPa, and the cold mass fractions of 0.5–0.7. Prabakaran and Vaidyanathan [19] investigated the effect of nozzle diameter on energy separation. Shamsoddini and Hossein Nezhad [20] numerically investigated the effects of nozzles number on the flow and power of cooling of a counter flow vortex tube. They concluded that as the number of nozzles is increased, power of cooling increases significantly while cold outlet temperature decreases moderately. Behera *et al.* [7] also studied the effect of nozzle shape and number numerically. All of implied investigations reported that the shape of inlet nozzles should be designed such that the flow enters tangentially into vortex tube chamber.

The flow patterns at the vortex chamber of the three CFD models of vortex tube, as the velocity field, are shown in fig. 6. Indeed, vortex chamber is a place that, cold exit is completely coincided to the end plan of its, but with smaller diameter than the main tube. In fig. 6a, in spite of 6 straight nozzles presence, locally injected momentum by means of nozzles in to vortex chamber is restricted to nozzle exit area only, that is instantaneously and low order because of small width of nozzle and division of total mass among the nozzles. What makes this set reasonable is only the creation of a symmetric flow field.

In fig. 6b, objection of locally momentum injection is recovered by increasing of nozzle width (nozzle area) because total nozzles area is constant for all of nozzles set. This situation caused a uniformly injection of momentum to produce semi continues high momentum zones in the rotating flow domain; as can be seen in the fig. 6b by red areas. It must be reminded that at this condition since the nozzles number is less than the last one, so the exit momentum from each nozzle is more effective to move downstream flow toward next nozzle.

Finally in fig. 6c, applying of 3 helical nozzles has removed the issue of instantaneously momentum injection and semi continues high momentum zones in the vortex chamber. These are implemented by formation of good tangential exit velocity from each helical nozzle. The properly exit swirl velocity, has provided a reasonable and interested rotating flow so that each nozzle gains sufficient enough energy to the downstream flow to push toward the next nozzle. These types of nozzles show that, they can produce somewhat higher swirl velocity than the others; as seen in fig. 7. Thus, it is a criterion to attain maximum cold temperature difference in the vortex tube device. It must be regard that in this condition the vortex tube has operated only with 3 helical nozzles instated of 6 straight nozzles.

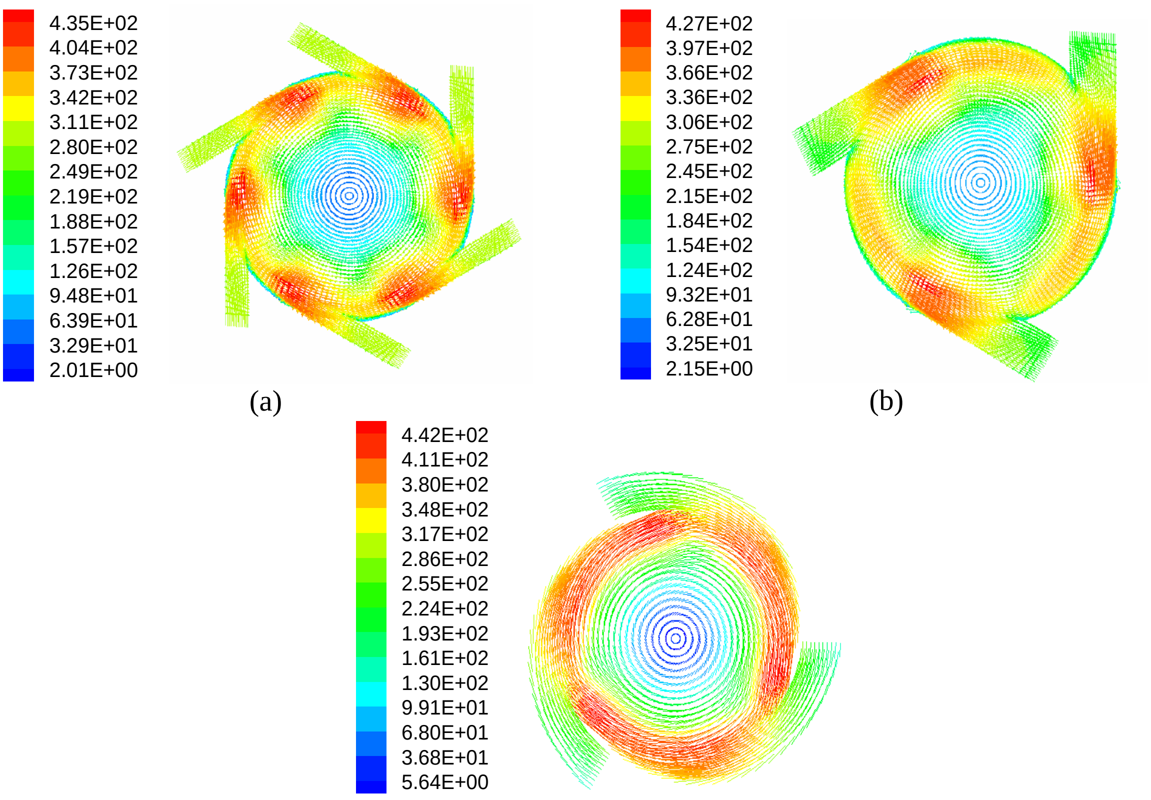

Figure 6. Velocity patterns at the vortex chamber obtained from CFD for a) 6 straight nozzles b) 3 straight nozzles c) 3 helical nozzles, α=0.3

Figure 7 illustrates the radial profiles for the swirl velocity at different axial locations. Comparing the velocity components, one can observe that the swirl velocity has greater magnitude of the axial velocity. The magnitude of the swirl velocity decreases as ever moves towards the hot end exit. The radial profile of the swirl velocity indicates a free vortex near the wall and becomes another type of vortex, namely forced vortex, at the core which is negligibly small according to the observations of Kurosaka [3].

Figure 8 shows the radial profiles of the axial velocity magnitude at different axial locations for specified cold mass fraction equal to 0.3. At the initial distances of tube, Z/L=0.1, cold gas has axial velocity greater than hot stream near the wall. Its maximum value occurs just in the centerline

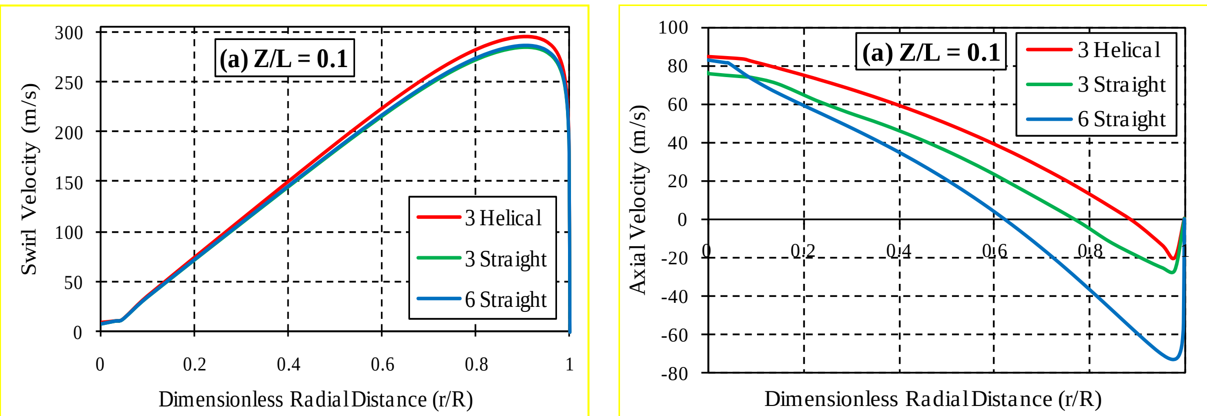

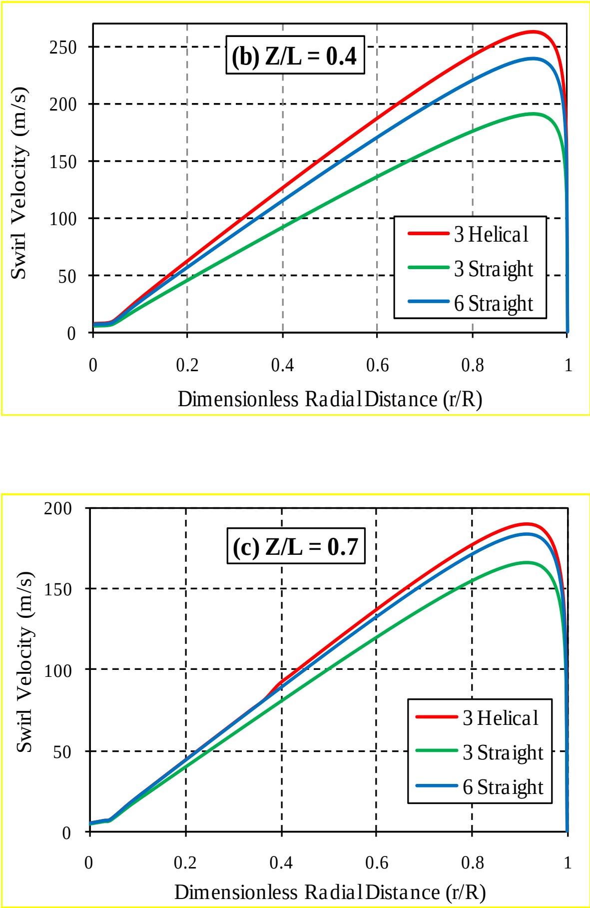

Figure 7. Radial profiles of swirl velocity at various axial positions, *α*=0.3

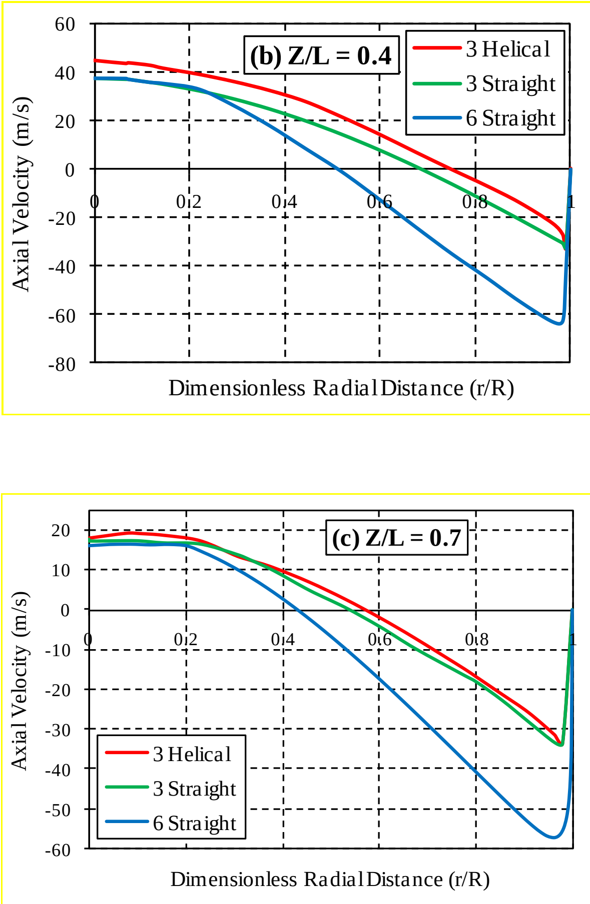

Figure 8. Radial profiles of axial velocity at various axial positions, *α*=0.3

and moves towards cold exit conversely to the hot flow which leaves the tube through the hot exit. In the higher values of dimensionless length *i.e.* Z/L=0.7, axial velocities of hot gas flow rises gradually in contrary to cold gas flow. The flow patterns relevant to 3 and 6 straight nozzles, have lead a cold temperature difference less than 3 helical nozzles. In comparison; however, the cold temperature difference of 3 straight nozzles has lower values than 6 straight nozzles, which would be expected. Table 2 summarized total temperature difference of cold and hot ends gases for various types of nozzles.

Table 2. Comparison of temperature difference for vortex tube with different nozzles, α=0.3

Model Type	Cold Exit Temperature (K)	Hot Exit Temperature (K)	$\Delta T_{i,c}$ (K)	$\Delta T_{i,h}$ (K)	$\Delta T_{c,h}$ (K)
3 helical	249.034	309.302	45.166	15.102	60.268
3 straight	255.124	304.837	39.076	10.637	49.713
6 straight	250.24	311.5	43.96	17.3	61.26

The vortex tube with 6 straight nozzles reaches hot and total temperature difference higher than 3 straight and 3 helical nozzles. However, if only the cold temperature difference is a criterion of well operating in that machine, 3 helical nozzles will provide good cooling condition. The total temperature distribution contours obtained from CFD analysis are plotted in fig. 9. It shows peripheral flow to be warmer and core flow colder relative to inlet temperature equals to 294.2 K, giving maximum hot gas temperature of 313.451 K and minimum cold gas temperature of 249.034 K for 3 helical nozzles.

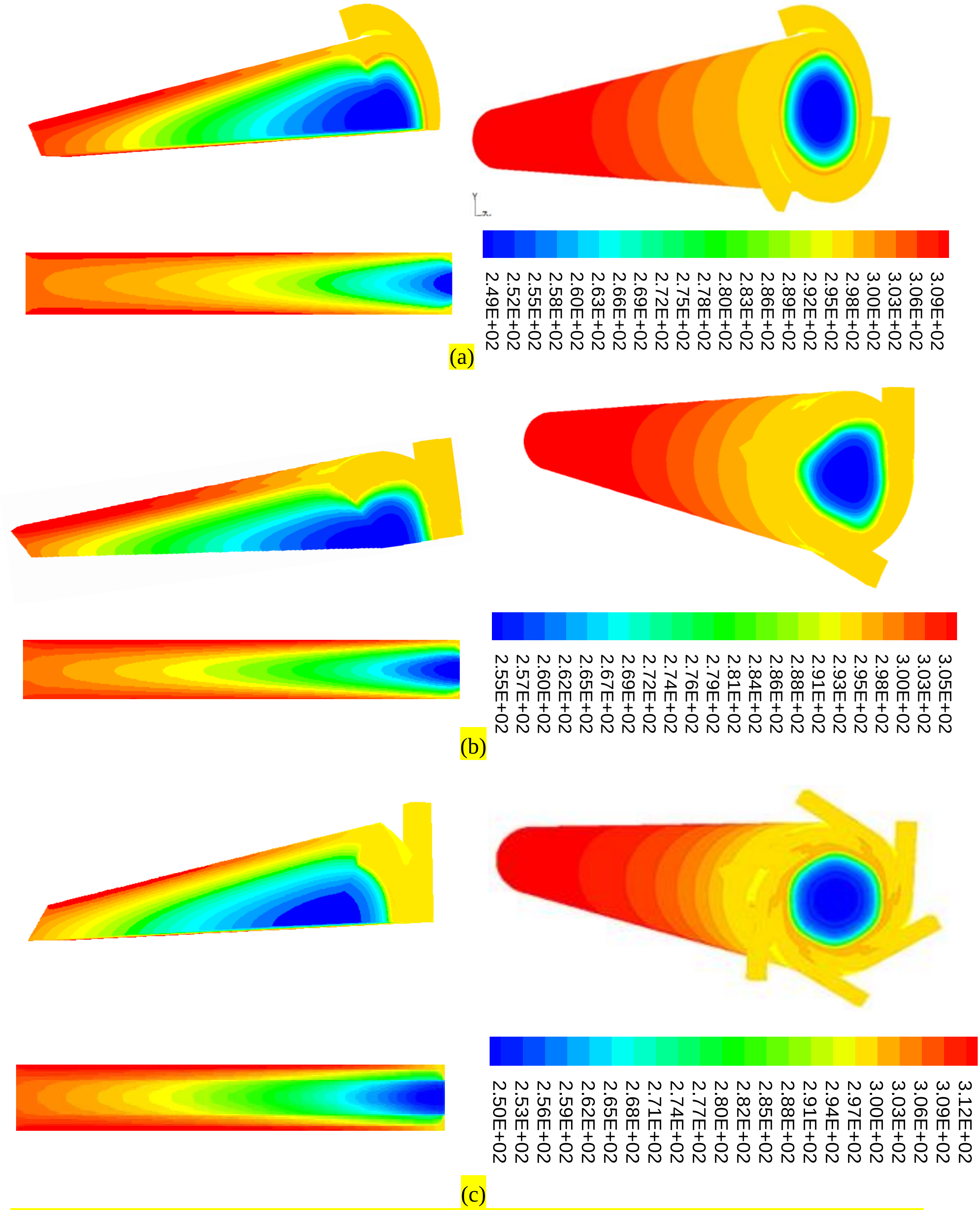

Figure 9. Temperature distribution in vortex tube with: a) 3 helical nozzles b) 3 straight nozzles c) 6 straight nozzles, α=0.3

Comparison of three different nozzles set in this figure, indicates that cold exit gas region in the 3 helical nozzles set is smaller than 3, and 6 straight nozzles vortex tube. This means that the mechanism of energy separation can occur just in a place that rotating flow has higher swirl velocity. Nevertheless, at the straight nozzles set the energy separation mechanism encountered with a considerable delay, which produces sufficient time to exchange of thermal energy between hot and cold cores. In addition, the flow patterns as path lines at sectional lengths near the cold, hot exits and mid region because of using different nozzles sets are shown in fig. 10. The formation of core and peripheral streamlines can be clearly seen at the near cold end and mid region, but after occurring of separation phenomenon the core vortex is disappeared. In spite of creating of such reverse flow, the peripheral flow does not alter its continuation toward the hot end. One should notice that, the axial distance between stagnation point and hot exit end is too short. The path lines help to realize of flow patterns, so that any flow filed symmetry, various regions of hot and cold flow can be identified by them. Approaching to a properly symmetric rotating flow and effective intensively domain can be seen in fig. 10a. The exact values of axial location for stagnation point due to utilize of any nozzles set will be presented and discussed at the following section in more details.

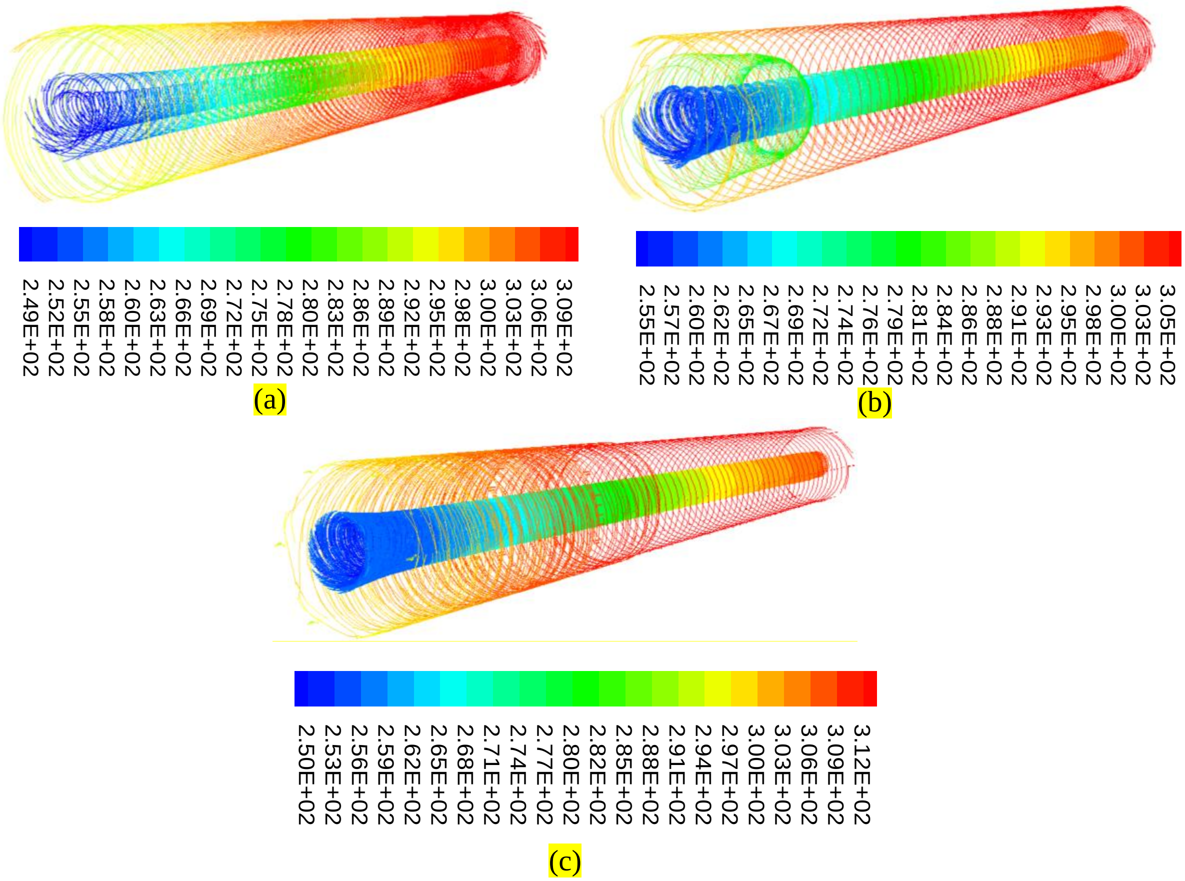

Figure 10. 3D Path lines colored by total temperature along the vortex tube with a) 3 helical b) 3 straight c) 6 straight nozzles, α=0.3

4.2 Power separation rate

The rate of energy (power) separation provides another measuring way for evaluation of the vortex tube performance. The rates of energy separation in the hot and cold exit streams ($\dot{Q}_c$ and $\dot{Q}_h$)

are determined and compared with the available experimental data of Skye *et al.* [8] as shown in fig. 11 and 12. The values of $\dot{Q}_c$ and $\dot{Q}_h$ can be evaluated as follows:

$$\dot{Q}_c = \dot{m}_c \, c_p (T_{in} - T_c) \tag{8}$$

$$\dot{Q}_h = \dot{m}_h \, c_p (T_h - T_{in}) \tag{9}$$

The helical nozzles set show a good capability of power separation rate in cold exit, however; the six straight nozzles reverse this phenomenon at the hot exit. Both the experimental data and the CFD models show maximum power separation with a cold fraction of about 0.65.

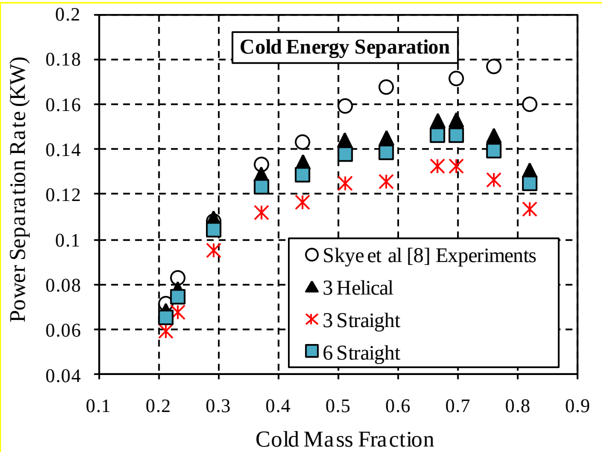

Figure 11. Comparison of cold power separation rate with experimental data

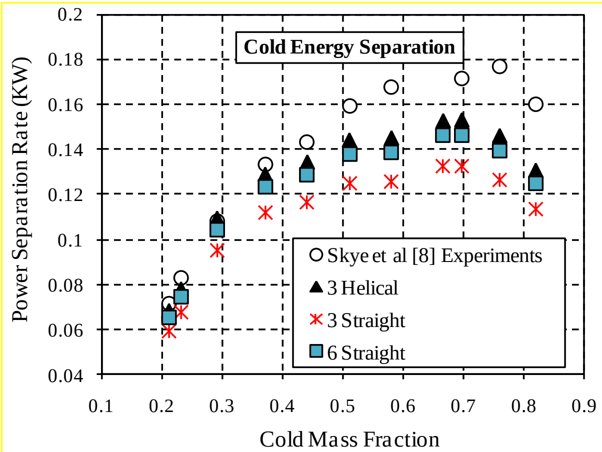

Figure 12. Comparison of hot power separation rate with experimental data

4.3 Stagnation point and wall temperature

Figure 13 attempts to clarify the reasons which make relationship between stagnation point position and where maximum wall temperature occurs. Physical mechanism of energy separation in vortex tube would be related to exist of two counter flows in the tube because of stagnation point presence [15], although these two locations are not exactly coincide to each other. The stagnation point position within the vortex tube can be determined by two ways: according to maximum wall temperature location, and on the basis of velocity profile along the tube length at the point where it ceases to a negative value. The point of maximum wall temperature represents the stagnation point determined by Fulton *et al*. [21]. Fulton stated that “at this point, the tube wall is hotter than the final mixed air and hotter than the tube wall either at the inlet or at the far end of the tube”. Figure 14 shows the stagnation point and corresponding streamlines in the r–z plane. The numerical results of Aljuwayhel *et al.* [6] CFD model, suggested that considerable or strictly spoken the most part of energy separation in the vortex tube occurs before stagnation point. At the present work, for the applied three set of nozzles, fig. 14 exaggeratedly illustrated axial difference of stagnation point along the tube.

Beside to attain maximum swirl velocity and maximum cold temperature difference, axial velocity distribution together with maximum wall temperature location also would be another two important parameters in designing of a good vortex tube. The former two criteria have been discussed in the previous sections, and resent parameters must be in reasonable conformity with them. So that

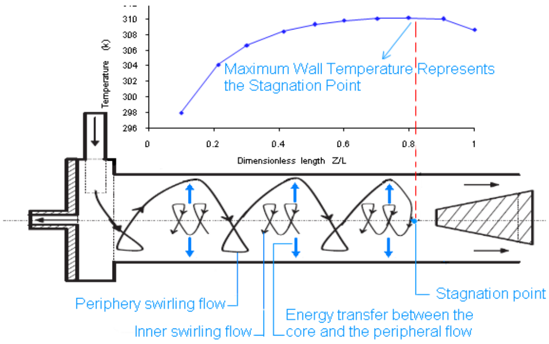

Figure 13. Schematic description of energy transfer pattern in the vortex tube

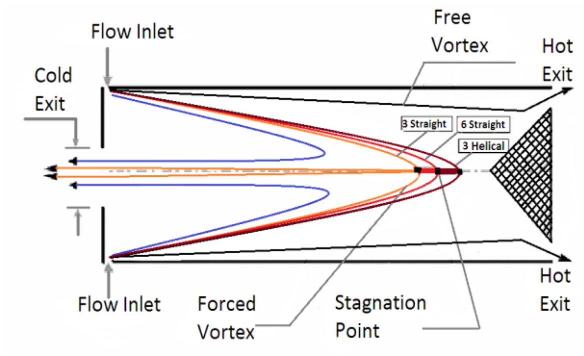

Figure 14. Exaggerated schematic drawing of separation point location for different nozzles

the present research would believe that the four mentioned facts should justify one another. The investigated variations of axial velocity along the center line of the vortex tube for 3 different type of nozzles set are shown in fig. 15, where the Z/L denoted as the dimensionless tube length. The results show that the positions of stagnation points for all of models are too close to the hot exit. But, 3 helical nozzles set causes the position of this point is drawn rather a little to the hot exit end. The axial locations of these pointes relative to hot exit end can be arranged as: first for 3 helical nozzles, second 6 straight nozzles and finally 3 straight, respectively. One can consider due to somewhat closeness of separation point of 3 helical nozzles set to the hot exit, it brings maximum cold temperature difference in this type of vortex tube. In other words, any nozzle shapes or their numbers that can produce a situation moving stagnation point possibly closer to hot exit would be preferred in comparison. Figure 16 depicts tube wall temperature distribution along a straight line laid from cold side to hot end.

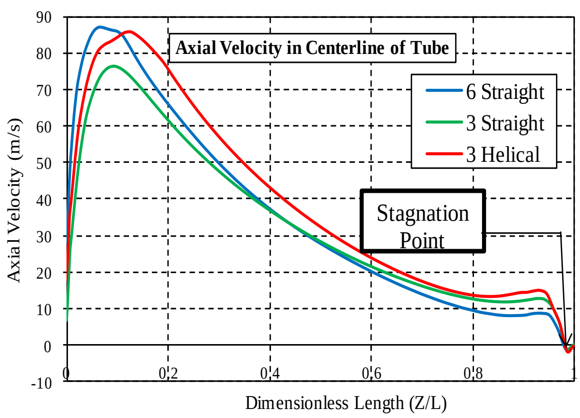

Figure 15. Variation of axial velocity along the center line of the vortex tubes

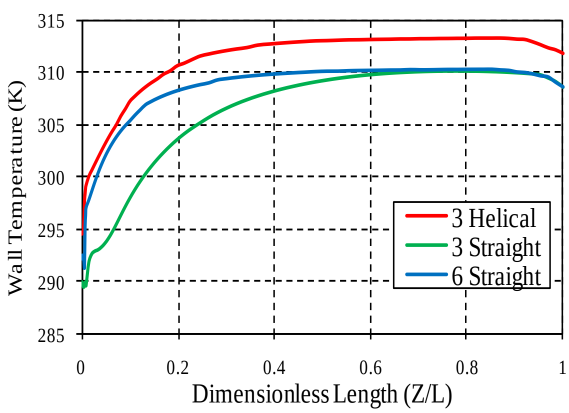

Figure 16. The variations of wall temperature along the vortex tubes length

As shown in fig. 7, the swirl velocities at the initial length of tube are very high. If one can accept that the large energy dissipation occurs just in this zone of high rotating flow field, thus sufficiently large temperature gradient would be expected, as shown in fig. 16. This condition has been continued until where is called stagnation point. Of course, these behaviors may be interpreted such that the needed length or control volume for dissipating of inlet flow kinetic energy is as small as for 3 helical nozzles. As a rough estimation, according to fig. 16, these dimensionless length are Z/L=0.18, Z/L=0.4 and Z/L=0.65, respectively. These arrangements lead to achieve greater wall temperature of 3 helical nozzles and then 6 straight nozzles relative to 3 straight nozzles. The evaluated numerical values for both $(Z/L)_w$ and $(Z/L)_v$ are compared in tab. 3. Also, as mentioned before; there is a slightly difference between maximum wall temperature and stagnation point axial locations. As illustrated in the fifth column of tab. 3, the 3 straight nozzles set devotes higher discrepancy itself.

Table 3. Comparison of the stagnation point location using two methods

Model	T_{wmax}	$(Z/L)_w$	$(Z/L)_v$	Diff%
3 Straight	310.101	0.816774	0.984	16.72
6 Straight	310.119	0.834784	0.985	15.2
3 Helical	313.402	0.869958	0.986	11.62

4.4 Secondary flow in helical nozzles

It is well-known that the secondary flow can developed in the curved/helical tubes, for example, Kurnia *et al.* [22] investigated the heat transfer performance of different geometry coils. They also studied secondary flow in curved shape tubes and its influence on the temperature distribution. In the proximity of curved ducts inner and outer walls, however, the axial velocity and the centrifugal force will approach zero. Hence, to balance the momentum transport, secondary flows will appear [22]. In the present research of helical nozzles, the formation of secondary flow is also investigated. Because of too short length of this type of nozzles, the flow stream does not have enough space and time for considerable secondary flow formation. However, as shown in fig. 17, secondary flow intensity grows up at the corners of nozzle duct. In this figure, the axial velocity profile in the plate near outlet of nozzle has been illustrated. Figure 18 depicts the predicted temperature distribution for the same plane of helical nozzle, which confirms a lower temperature gradient in the nozzles.

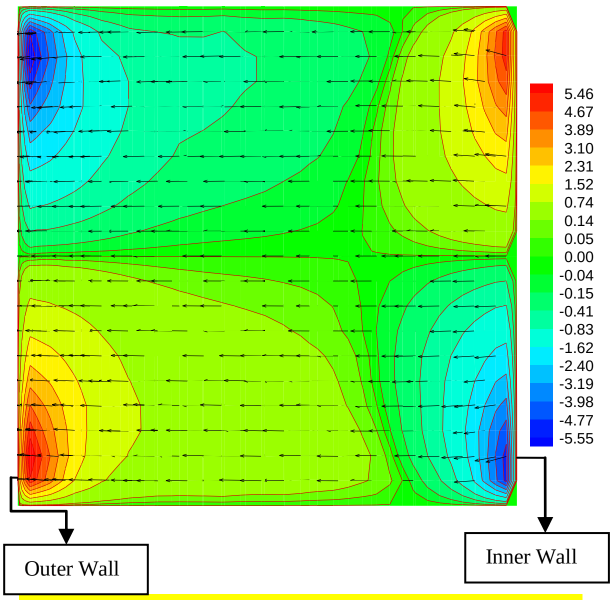

Figure 17. Axial velocity profile of air flow in a helical rectangular cross section nozzle

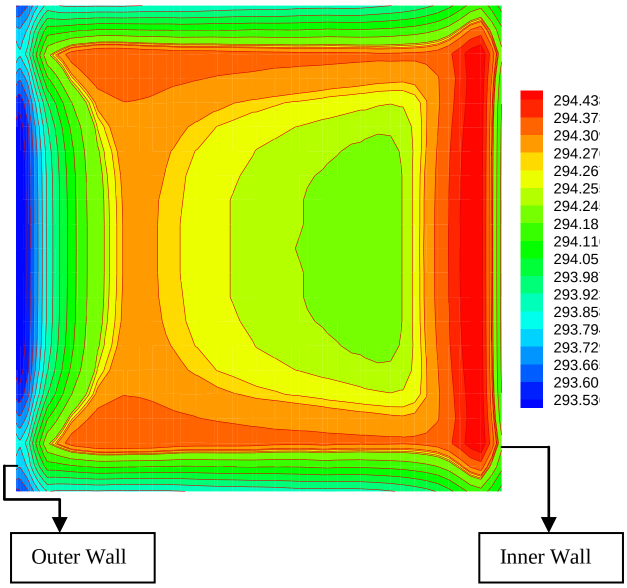

Figure 18. Temperature distribution of air flow in a helical rectangular cross section nozzle

Formation of secondary flow causes slightly increasing of gas temperature near inner wall, and as expected affects negligibly the heat transfer performance. Consequently, because of weak formation of secondary flow in this nozzles set, then, it is assumed that it cannot influence the vortex tube flow behavior.

Application of vortex tube device showed that this machine does not have engineering justification, and attaining to maximum cold exit temperature is only important criterion. This paper has endeavored on the ways which can help to this demand. Of course, effect of pressure drop in the nozzles is one of the important facts. In this way, both pressure drop and the thermal energy separation per unit pumping power/pressure drop in terms of Figure of Merit are investigated in the present article, and these results are shown in fig. 19 and 20.

According to the obtained results of fig. 19, it is obvious that helical nozzles set has higher pressure drop than straight ones. By analyzing of results of fig. 20, respect to Figure of Merit criteria; one can accept that straight nozzles set helps to decrease of pressure drop.

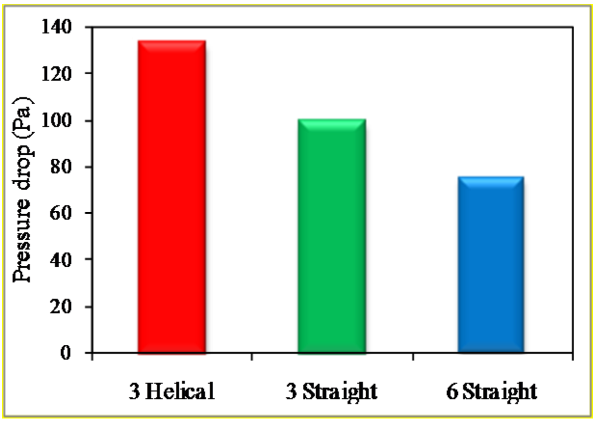

Figure 19. Pressure drop in the three different set of nozzles

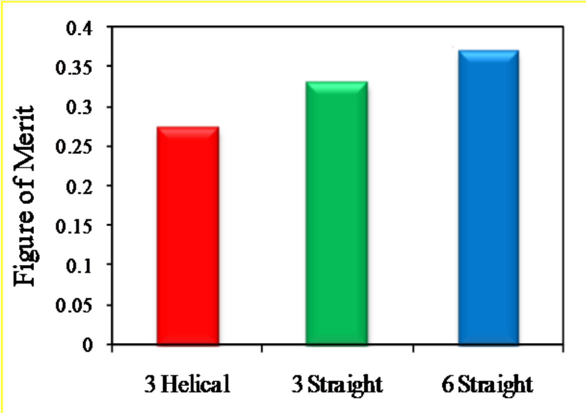

Figure 20. Figure of merit of different nozzle types

However, straight geometry is not suitable to produce reasonable swirl velocity (or equally thermal energy separation) in the vortex chamber. On the other hand, because of flow field complexity in vortex tube an expectation on the nozzle function is merely focused on the capability of producing higher values of swirl velocity; that is implemented by helical nozzles.

Conclusion

A computational approach has been carried out to realize the effects of injection nozzles shape and its number on the performance of vortex tube. In a three dimensional compressible flow, standard k-ε turbulence model is employed to analyze the flow patterns through the CFD models. Three nozzles set consist of 6 straight, 3 straight and 3 helical nozzles have been studied. The main purpose was considered to reach maximum cold temperature difference. In this way, numerical results shown that higher swirl velocity due to appropriately nozzles shape can effectively influence the exit cold gas temperature. Comparison of flow fields in the three nozzles sets has been cleared that helical nozzles are suitable to the desired amount of energy separation and higher cold gas temperature difference.

Using of 6 straight nozzles, have locally injected momentum to fluid flow in the vortex chamber. This is not sufficient because in this case increased momentum of flow is restricted only in a small region just at vicinity of nozzles exit area. In utilizing of 3 straight nozzles the exit area is increased, thus a semi continues high momentum regions are created in the rotating flow field domain. However, 3 helical nozzles set has removed objections of the last two sets, since a good tangential exit velocity from the helical nozzles is provided. Hence, each nozzle helps to gain sufficient energy to the downstream flow in order to conduct them toward next nozzle.

Moreover, this conclusion has also been proven by investigating of another four facts. These criteria are maximum cold temperature difference, capability of swirl velocity increasing, location of stagnation point, which occurs in a place that is farther than cold exit and finally adjustment possibility between the locations of maximum wall temperature with stagnation point position. The total temperature separations (hot and cold exit) predicted by the CFD model of 6 straight nozzles were found to be in a good agreement with available experimental data and another flow characteristics shown reasonable behaviors.

Nomenclature

D	-Diameter of vortex tube [mm]
k	-Turbulence kinetic energy [$m^2\ s^{-2}$]
L	-Length of vortex tube [mm]
R	-Radial distance measured from the centerline of tube [mm]
T	-Temperature [K]
T_{wmax}	-Maximum wall temperature [K]
Z	-Axial length from nozzle cross section [mm]
$(Z/L)_w$	-Axial location of maximum wall temperature
$(Z/L)_v$	-Axial location of stagnation point

Greek Symbols

α	-Cold mass fraction
ε	-Turbulence dissipation rate [$m^2\ s^{-3}$]
$\Delta T_{c,h}$	-Temperature difference between cold and hot end [K]
$\Delta T_{i,c}$	-Temperature difference between inlet and cold end [K]
$\Delta T_{i,h}$	-Temperature difference between hot end and inlet [K]
ρ	-Density [$kg\ m^{-3}$]
σ	-Stress [$N\ m^{-2}$]
μ	-Dynamic viscosity [$kg\ m^{-1}\ s^{-1}$]
μ_t	-Turbulent viscosity [$kg\ m^{-1}\ s^{-1}$]
τ	-Shear stress [$N\ m^{-2}$]
τ_{ij}	-Stress tensor components

References

[1] Ranque, G.J., Experiences sur la détente giratoire avec simultanes d'un echappement d'air chaud et d'un enchappement d'air froid, *J. Phys.Radium*, 4 (1933), pp. 112-114

[2] Hilsch, R., Die expansion von gasen im zentrifugalfeld als kälteproze, *Z. Naturforschung* 1(1946), pp. 208-214

[3] Kurosaka, M., Acoustic Streaming in Swirling Flows, *J. Fluid Mech*., 124 (1982), pp. 139-172

[4] Stephan, K., *et al*., An Investigation of Energy Separation in a Vortex tube, *Int. J. Heat Mass Transfer*, 26 (1983), pp. 341-348

[5] Ahlborn, B., Gordon, J., The Vortex Tube as a Classical Thermodynamic Refrigeration Cycle, *J. Appl. Phys*, 88 (2000), pp. 645-653

[6] Aljuwayhel, N.F., Nellis, G.F., Klein, S.A., Parametric and Internal Study of The Vortex Tube Using a CFD Model, *Int. J. Refrig*., 28 (2005), pp. 442-450

[7] Behera, U., *et al*., CFD Analysis and Experimental Investigations Towards Optimizing The Parameters of Ranque-Hilsch Vortex Tube. *Int. J. Heat and Mass Transfer*, 48 (2005), pp. 1961-1973

[8] Skye, H.M., Nellis, G.F., Klein, S.A., Comparison of CFD Analysis to Empirical Data in a Commercial Vortex Tube. *Int. J. Refrig*., 29 (2006), pp. 71-80

[9] Chang, H.S., Experimental and Numerical Studies in a Vortex Tube, *Journal of Mechanical Science and Technology*, 3 (2006), pp. 418-425

[10] Eisma., Promvonge, S., Numerical Investigations of The Thermal Separation in a Ranque-Hilsch Vortex Tube. *Int. J Heat and Mass Transfer* , 50 (2007), pp. 821-32

[11] Kirmaci V., Optimization of Counter Flow Ranque-Hilsch Vortex Tube Performance Using Taguchi Method, *International Journal of Refrigeration*, 32 (2009), pp. 1487-1494

[12] Akhesmeh, S., Pourmahmoud, N., Sedgi, H., Numerical Study of the Temperature Separation in the Ranque-Hilsch Vortex Tube, *American Journal of Engineering and Applied Sciences*, 3 (2008), pp. 181-187

[13] Xue, Y., Ajormandi M., Kelso, R., A Critical Review of Temperature Separation in a Vortex Tube, *Journal of Experimental Thermal and Fluid Science*, 8 (2010), pp. 1367-1374

[14] Bramo, A.R., Pourmahmoud, N., A Numerical Study on The Effect of Length to Diameter Ratio and Stagnation Point on The Performance of Counter Flow Vortex Tube, *Aust. J. Basic & Appl. Sci*., 4 (2010), pp. 4943-4957

[15] Bramo, A.R., Pourmahmoud, N., CFD Simulation of Length to Diameter Ratio Effect on The Energy Separation in a Vortex Tube, *Thermal Science*, In Press

[16] Pourmahmoud, N., Bramo, A.R., The Effect of L/D Ratio on The Temperature Separation in The Counter Flow Vortex Tube , *IJRRAS*, 6 (2011), pp. 60-68

[17] Hossein Nezhad, A., Shamsoddini, R., Numerical Three-Dimensional Analysis of The Mechanism of Flow and Heat Transfer in a Vortex Tube , *Thermal Science*, 4 (2009), pp. 183-196

[18] Kirmaci, V., Uluer, O. An Experimental Investigation of the Cold Mass Fraction, Nozzle Number, and Inlet Pressure Effects on Performance of Counter Flow Vortex Tube, *Journal of Heat Transfer*, 131 (2009), pp. 603-609

[19] Prabakaran, J., Vaidyanathan S., Effect OF Diameter of Orifice and Nozzle on the Performance of Counter Flow Vortex Tube, *International Journal of Engineering Science and Technology*, 4 (2010), pp. 704-707

[20] Shamsoddini, R., Hossein Nezhad, A., Numerical Analysis of The Effects of Nozzles Number on The Flow and Power of Cooling of a Vortex Tube, *International Journal of Refrigeration*, 33 (2010), pp. 774-782

[21] Fulton, C.D., Ranque's tube, *J Refrig Eng.*, 5 (1950), pp. 473-479

[22] KURNIA, J.C., SASMITO. A.P., MUJUMDAR. A.S., Laminar Convective Heat Transfer for In-Plane Spiral Coils of Non-Circular Cross Section Ducts: A computational fluid dynamics study, *Thermal science*, (2011), in press